Chapter 3
Multimodality Imaging of the Right Heart

Edith Liliana Posada-Martinez, Xochitl A. Ortiz-Leon, Lissa Sugeng, and David J. Hur

Case

A 29-year-old gentleman presented with atypical chest pain associated with shortness of breath, but no nausea or diaphoresis. He also reported a history of palpitations since age 16, but no cyanosis. Physical exam revealed normal rate, regular rhythm with widened split S1, a 2/6 early systolic ejection murmur at the mid sternal border, and no gallop or friction rub. His abdomen was normal. Examination of his extremities revealed no signs of cyanosis or edema. Electrocardiogram was normal sinus rhythm with incomplete right bundle branch block, troponin within reference range, and chest radiograph showed cardiomediastinal silhouette within normal limits.

In the course of his workup, he underwent transthoracic echocardiogram (TTE) that demonstrated blood flow through mainly the upper portion of the interatrial septum, suggesting

David J. Hur, MD, FACC is an US Government employee.

E. L. Posada-Martinez · X. A. Ortiz-Leon · L. Sugeng · D. J. Hur (✉)
Section of Cardiovascular Medicine, Department of Internal Medicine, Yale School of Medicine, New Haven, CT, USA
e-mail: edith.posadamartinez@yale.edu; xochitl.ortizleon@yale.edu; lissa.sugeng@yale.edu; david.hur@yale.edu

L. Tsao, M. E. Afari (eds.), *Clinical Cases in Right Heart Failure*, Clinical Cases in Cardiology,
https://doi.org/10.1007/978-3-030-38662-7_3

a wide atrial septal defect (ASD) with superior extension (Fig. 3.1a) and concern for minimal to no tissue rim at the superior aspect; the right ventricular systolic pressure (Fig. 3.1b) was 28 mmHg (including a right atrial pressure of 5 mmHg). The right ventricle (RV) appeared mildly dilated (diastolic internal diameter 4.5 cm and indexed 2.25 cm/m^2) but still with preserved function (Figs. 3.2 and 3.3).

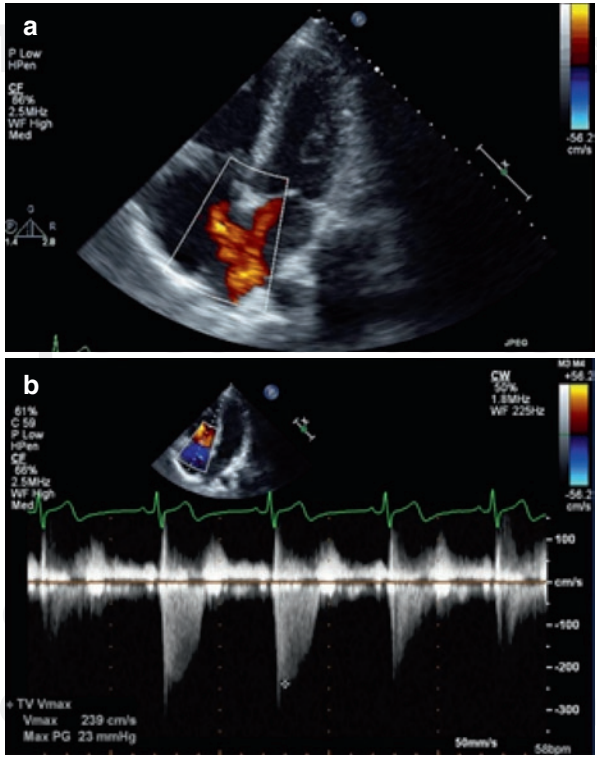

Figure 3.1 (**a**) Modified four-chamber view showing the atrial septal defect with colour Doppler flow coming from left atrium into right atrium. (**b**) Continuous-wave Doppler of tricuspid regurgitant jet for calculating the right ventricular systolic pressure by modified Bernoulli equation (23 mmHg), plus estimated right atrial pressure 5 mmHg, to get 28 mmHg

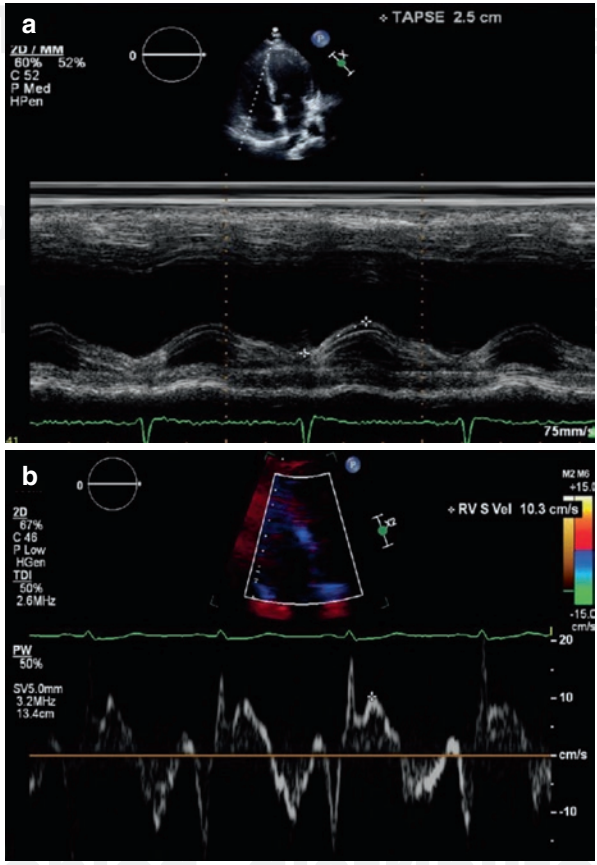

FIGURE 3.2 (**a**) Tricuspid annular plane systolic excursion (TAPSE) >1.7 cm. (**b**) Doppler tissue imaging-derived tricuspid lateral annular systolic velocity wave (S′) >9.5 cm/s

Because of the importance of the anatomic evaluation of the defect, the patient underwent cardiovascular magnetic resonance (CMR) imaging, which visualized a secundum ASD seen in the superior portion of the interatrial septum (Fig. 3.4). The ASD measured 1.4 cm in the superior-inferior axis (Fig. 3.5); there was approximately half a centime-

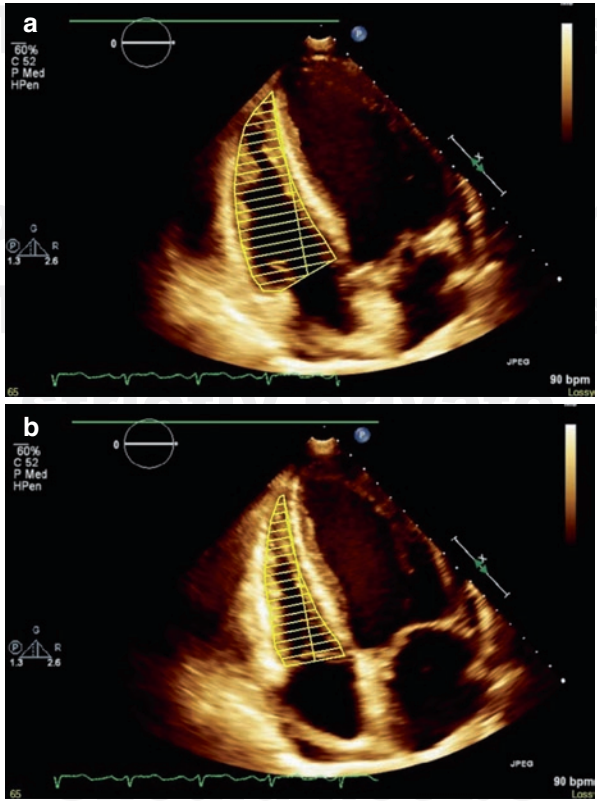

FIGURE 3.3 Fractional area change (FAC) >35%. (**a**) End-diastolic area. (**b**) End-systolic area

tre of surrounding tissue rim superiorly and the Qp:Qs was 2.3:1 (Fig. 3.6), consistent with a hemodynamically significant left-to-right shunt. The systemic and pulmonary venous return was normal. There were no atrioventricular or ventricular defects found. There was moderately enlarged right ventricular size (end-diastolic volume 342 mL and indexed 173 mL/m^2) with normal right ventricular systolic function

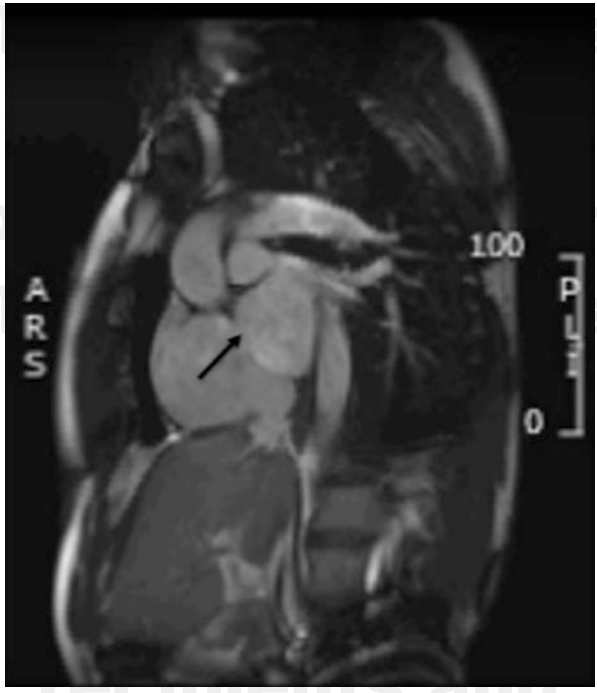

FIGURE 3.4 Cine imaging in the short-axis orientation at the level of the atria depicts the secundum atrial septal defect (arrow) with a small rim of superior septal tissue that was sufficient for placement of percutaneous septal occluder device

with right ventricular ejection fraction (RVEF) of 52%. Tricuspid regurgitation (TR) was mild (regurgitant fraction 14%), and right atrium (RA) was moderately enlarged. There was no delayed enhancement.

Given that there was a sizeable ASD with hemodynamic left-to-right shunting with enlarged right heart size but still normal right ventricular function, it was felt that it was time to intervene, and close the defect before the development of

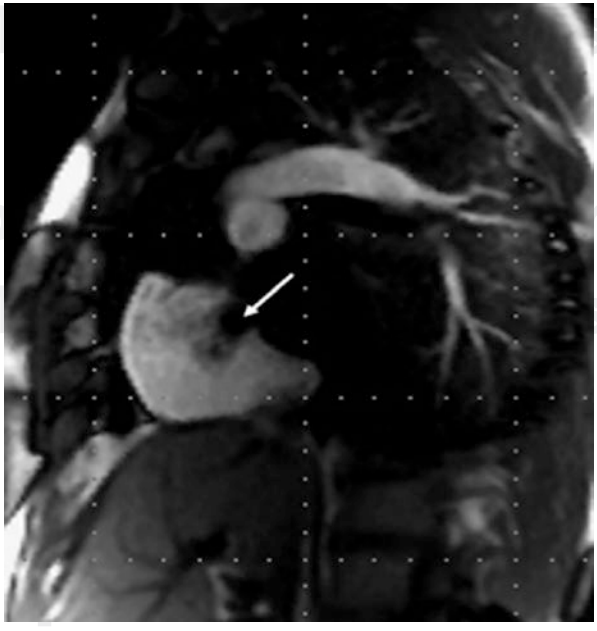

FIGURE 3.5 First-pass perfusion imaging with real-time injection of contrast depicts the ASD (arrow) with left-to-right shunting (non-contrast-mixed blood from the left atrium shunting across the ASD to the right atrium containing contrast-mixed blood, yielding a "negative contrast" void). The length of the ASD measures up to 1.4 cm

right ventricular dysfunction and subsequent right heart failure. The patient underwent transoesophageal echocardiogram (TOE) in order to characterize the defect and assess if he was a candidate for a percutaneous septal occluder device. The TOE confirmed a large secundum ASD, measuring 5 × 2.5 cm with adequate tissue rim at the superior aspect. He was referred to the Structural Heart Interventional Cardiology team for closure.

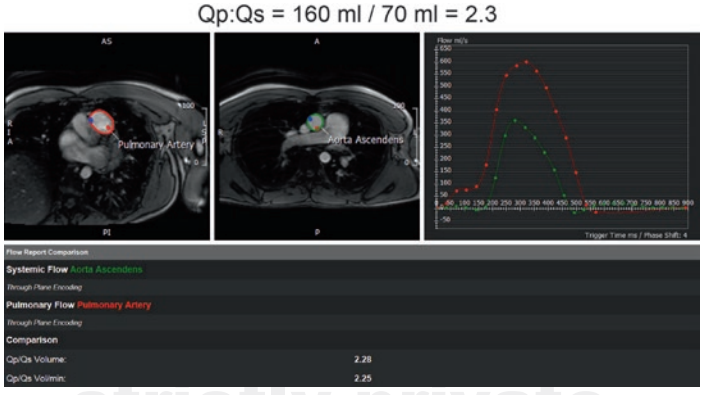

FIGURE 3.6 PC-CMR performed in the pulmonary artery (red contour) and the ascending aorta (green contour) to measure the respective flows. There was no significant pulmonic or aortic regurgitation. The absolute flow detected in the pulmonary circulation as evidenced in the pulmonary artery (Qp) is 160 mL and in the systemic circulation as evidenced in the ascending aorta (Qs) is 70 mL. Thus, the ratio (Qp:Qs) is 160 mL/70 mL, which is 2.3, signifying a significant left-to-right shunt

3.1 Echocardiographic Assessment of RV Function

3.1.1 RV Systolic Function

The complex crescent shape of the RV hinders its evaluation, therefore in some cases a multimodality approach with echocardiography, cardiac computed tomography and CMR is required. The echocardiogram is the first step in the imaging evaluation of right heart pathology [1]. The systolic function of the RV is an important parameter in clinical practice that has shown its usefulness in the whole spectrum of cardiac

pathology: ischemic cardiomyopathy, non-ischemic heart failure, congenital heart disease, and pulmonary hypertension (PH), as well as prior to cardiac surgery, and in recent years, percutaneous transcatheter cardiac interventions [2, 3].

The systolic function of the RV can be evaluated through different echocardiographic parameters; including tricuspid annular plane systolic excursion (TAPSE), RV myocardial performance (RIMP) or Tei index, fractional area change (FAC), Doppler tissue imaging (DTI)-derived tricuspid lateral annular systolic velocity wave (S′), and with novel echocardiographic techniques such as global longitudinal strain (GLS) and three-dimensional (3D) RVEF [1, 4].

The TAPSE represents a measure of RV systolic longitudinal function. According to the recommendations, it is measured in the apical RV-focused four-chamber view [5] by M-mode with the cursor positioned in the tricuspid lateral annulus; it measures the distance between end-diastole and peak systole in millimetres. TAPSE is a straightforward parameter that is easy to perform; however, it is angle-dependent and may be affected by the cardiac translation. The cut-off value for RV dysfunction by TAPSE is <17 mm [4].

Similarly to TAPSE, peak systolic velocity of tricuspid annulus (S′) is a measure of the systolic longitudinal function of the RV. S′ is measured from the apical four-chamber view by pulsed-wave DTI in cm/sec. This parameter is also easy to measure and reproducible, but it has the main disadvantage of being angle-dependent [4]. An S′ velocity <9.5 cm/s indicates RV systolic dysfunction.

The FAC is the percentage of area change in systole with respect to diastole and is also measured in a RV-focused apical four-chamber view. It is calculated subtracting end-systolic area (ESA) from end-diastolic area (EDA) divided by EDA: FAC = [(EDA – ESA)/EDA] × 100. This parameter includes the longitudinal and radial function of the RV. Thus, it is considered a parameter of global systolic function. This is still a single-plane measure of the RV function and has a fair inter-observer reproducibility. A value <35% indicates systolic dysfunction of the RV [4].

The RIMP or Tei index can be measured using either pulsed-wave (PW) spectral Doppler or DTI velocity of the lateral tricuspid annulus. It is calculated by adding the isovolumic contraction time (IVCT) to the isovolumic relaxation time (IVRT) divided by the ejection time (ET) interval: RIMP = [(IVCT + IVRT)/ET]. This parameter is considered also a measure of global RV performance since it includes parameters of systolic function and also the isovolumic relaxation. A RIMP >0.43 by PW Doppler and >0.54 by DTI suggests RV dysfunction. Tei index is unreliable when the right atrium (RA) pressure is high, which will shorten the IVRT [4].

The rate of increase in ventricular pressure (dP/dt) is a contractility index, which measures the rate of increase in the ventricle's pressure during the period of isovolumic contraction, when atrial pressure remains relatively constant and changes in the regurgitant flow velocity reflects the ventricular contractility [6]. In the right side, dP/dt measures the time required for the TR velocity to increase from 1–2 m/s. The increase in pressure (dP) is calculated using the modified Bernoulli principle ($P = 4\ V^2$), where V is the maximal velocity of the TR jet in meters per second (m/s); therefore $4\ (2)^2 = 16$ and $4(1)^2 = 4$, so dP = 16–4; dP = 12 mmHg. The time interval (dt) is measured between 1 and 2 m/s. Finally, the dP/dt is calculated as 12 mmHg divided by this time (in seconds). The recommendation for dP/dt of the RV has been defined as the lower normal limit to be approximately 400 mmHg/s [1, 7]. The main limitation of this parameter is its load-dependency.

3.1.2 RV Diastolic Function

The parameters for the assessment of the RV diastolic function are basically those used for the left side; however, important considerations should be addressed. The parameters should be acquired from the apical four-chamber view and must be taken at held expiration or the average of at least five consecutive beats due to respiratory variation. Moreover, these parameters can be affected by age, respiration, heart rate, and loading

conditions. Assessment of RV diastolic function is carried out by pulsed Doppler of the tricuspid inflow (E and A waves), tissue Doppler of the lateral tricuspid annulus (e′ and a′ waves), pulsed Doppler of the hepatic vein, and measurements of IVC size and collapsibility. The quantification of RV diastolic function include the following parameters: E/A ratio (1.4 ± 0.3), E wave deceleration time (180 ± 31 ms), e′/a′ ratio (1.18 ± 0.33), e′ (14.0 ± 3.1 cm/s) and E/e′ ratio (4.0 ± 1.0) [4]. In addition, estimation of RA pressure by measurement of IVC diameter and collapse with inspiration should be considered in the determination of RV diastolic function. According to guidelines for the echocardiographic assessment of the right heart in adults by the American Society of Echocardiography, the RV diastolic dysfunction should be graded as follows: tricuspid E/A ratio <0.8 suggests impaired relaxation, a tricuspid E/A ratio of 0.8–2.1 with an E/e′ ratio >6 or diastolic flow predominance in the hepatic veins suggests pseudonormal filling, and a tricuspid E/A ratio >2.1 with a deceleration time <120 ms suggests restrictive filling [1].

There are few studies that have evaluated the clinical impact of RV diastolic dysfunction. The E/e′ has a high sensitivity and specificity for predicting RA pressure ≥10 mmHg in non-cardiac surgery and in cardiac transplantation [8, 9]. In patients with PH and chronic heart failure, diastolic dysfunction was associated with worse functional class and was an independent predictor of mortality [10, 11]. In addition, diastolic RV dysfunction may be considered a marker of early RV dysfunction because it is often present before systolic function drops [1].

3.2 Echocardiographic Assessment of RV Size and Hemodynamics

3.2.1 RV Chamber Assessment

The RV is a crescent-shaped structure, anteriorly located, and smaller than the left ventricle but with a thinner free wall that

receives venous circulation through the vena cava and continues with the pulmonary artery [12, 13]. The RV is divided in three components based on their embryological origins: the inlet (which includes tricuspid valve, tendinous chords, and papillary muscles); the apex (a portion very trabeculated); and the infundibulum or conus (which includes the pulmonary valve). The crista supraventricularis separates the RV inlet and outlet portions.

Unlike the left ventricle, the RV has only two myocardial layers, the superficial and subendocardial. The superficial RV layer (approximately 25% of wall thickness) is arranged circumferentially in a parallel direction with the atrioventricular groove, and extends toward the left ventricle and contributes along with the septum to the biventricular interdependence [14]. On the other hand, the subendocardial RV layer (approximately 75% of wall thickness) has the myocytes arranged in a longitudinal direction and contributes in greater proportion to the systolic function of the RV [14, 15].

Because of the complexity of the RV geometry, the RV size is often evaluated by conventional 2D echocardiography through multiple acoustic windows; however, the accuracy of these parameters may be limited when the free wall is not well defined, such as in patients with dilated RVs. RV-focused apical four-chamber view is considered the best approach for these measurements. Recent studies have shown ultrasound enhancing agents improve the visualization of RV endocardial borders by decreasing inter-observer variability and resulting in more accurate evaluation of RV size and function [16, 17]. The reference values commonly used in 2D echocardiography to indicate RV dilation are: diameter >41 mm at the base and >35 mm at the midlevel in the RV-focused four-chamber view [4].

3.2.2 *Right Heart Pressures Assessment*

Echocardiography allows estimation of the right ventricular systolic pressure (RVSP), which in the absence of pulmonary stenosis will be the same as pulmonary artery systolic pressure

(PASP). The RVSP is determined from the TR jet using continuous-wave Doppler plus the right atrial pressure (RAP). The peak pressure gradient (ΔP) is calculated through the modified Bernoulli equation: $\Delta P = 4 V^2$ as described above [1]. The RAP is determined by the diameter of the inferior vena cava (IVC) evaluated in a subcostal view, 1–2 cm from the IVC-RA junction and its percentage of collapsibility during an inspiratory sniff [4]. According to these parameters the values for the RAP are as follows: IVC diameter <2.1 cm with collapse >50% suggest mean RAP of 3 mm (range between 0 and 5 mmHg); IVC diameter >2.1 cm with collapse <50% suggests mean RAP of 15 mmHg (range between 10 and 20 mmHg); for the remaining combinations an intermediate mean value of 8 mmHg (range between 5 and 10 mmHg) may be assumed.

3.3 Novel Echocardiographic Assessment of the RV

3.3.1 Speckle Tracking/Strain

The study of myocardial fibers has been carried out with different techniques by echocardiography. Nowadays, the most widely used technique is speckle tracking on the basis of displacement measurements. Speckle tracking analyses different parameters of cardiac mechanics such as displacement, velocity, strain, and strain rate. Strain is the fractional change in the length of a myocardial segment, expressed as a percentage, unitless, and can analyse these changes in the longitudinal, circumferential, and radial direction. The GLS, which is the average of the segmental strain, is the parameter most widely used and has shown the most clinical implications [18]. The RV GLS, measured in the RV-focused four-chamber view, is calculated as the average of the three segments of the free wall (basal, mid, and apical) or can include the three segments of the septal wall and be calculated as the average of the six segments. Most of the studies showing the clinical applications of RV GLS measured the free wall longitudinal

strain (FWGLS) because it is considered that the septal wall is mostly affected by LV mechanics; however, both methods seem to have excellent agreement [19]. This technique is considered angle-independent and reproducible, but it is influenced by load conditions, image quality, and artefacts. An important limitation for this technique is the variability among vendors and the lack of multiple studies with larger populations to determine normal values [20, 21]. The current cutoff value established by the guidelines for RV GLS is >−20 (<20 magnitude with the negative sign) [4].

RV strain has shown prognostic value in different clinical scenarios such as heart failure [22–24] or myocardial infarction [25, 26]. In the PH setting, a RV GLS <10% of the basal segment of the RV free wall was a predictor of poor prognosis [27]. In addition, RV strain predicts RV failure after extracorporeal membrane oxygenation [28] as well as being a predictor of worse outcomes in patients who undergo cardiac surgery [29, 30].

3.3.2 3D Echocardiography

Although the above mentioned parameters have shown their usefulness in assessing and predicting outcomes in different cardiac pathologies, they are based on geometrical assumptions of the RV and do not include the complete analysis of all parts of the RV (inlet, apex, and the infundibulum). The TAPSE, S′, RIMP, and RV FWGLS are focused on the longitudinal function and lacking in the evaluation of transverse (radial) function. On the other hand, the FAC can determine the RV function in both directions; however, it does not include the infundibular portion of the RV, which accounts for around 20% of the end-diastolic volume [31]. So far 3D echocardiography has become the most accurate tool for the evaluation of RV function and has been validated against CMR, which is considered the gold standard for measuring volumes and EF [32]. Despite this, few studies have analysed the clinical

impact of 3D RV volumes and RVEF [33, 34]. This may be due to less availability of the software and the lack of training in the acquisition and analysis of 3D data. Nevertheless, 3D RV analysis is a promising tool in patients with right heart disease.

3.4 The Role of Cardiac MRI in Investigating the RV

3.4.1 Function/Volume Assessment

CMR is a non-invasive 3D tomography technique considered the standard of reference for the evaluation of cardiac volumes and systolic function [35]. In the right heart, CMR has demonstrated to be accurate and reproducible for the quantification of RV function including volumes and EF [36–38]. In addition, CMR allows for the assessment of morphology, quantification of RV mass, tissue characterization and valvular function through the analysis of transvalvular flows [39, 40].

In general, CMR scans include different phases. First, the cine sequence allows the assessment of morphology and the calculation of volumes, size, and EF [41]. Next, the phase contrast (PC) is useful in the analysis of valvular function such as quantification of TR or pulmonic regurgitation (PR) severity. Ultimately, post-contrast sequences can be performed. Delayed enhancement with gadolinium (DEG) imaging is a very useful technique that can evaluate myocardial scar or fibrosis [35].

CMR cine imaging allows hemodynamic evaluation of the RV through the quantification of end-diastolic, end-systolic, and stroke volumes, and ultimately RVEF. Additionally, right-sided cardiac output can be calculated by multiplying the stroke volume by the heart rate. Cine imaging allows for evaluation of right heart morphology and identification of RV hypertrophy [36], RA enlargement [42], and RV wall motion abnormalities. For example, in

patients with inferior myocardial infarction with extension to the RV or septal abnormalities due to volume overload (flattening or leftward bowing during diastole) or pressure overload (flattening or leftward during systole) that may suggest associated PH. Septal bowing is indicative of PASP ≥67 mmHg, leading to impaired filling and reduced LV end diastolic volume and decreased cardiac output [42, 43]. The RV volumes measured by CMR are an important predictor of outcomes in patients with right side pathology [44]. For example, patients with repaired tetralogy of Fallot, who frequently have PR, severe RV dilation (RV end-diastolic volume index ≥160 mL/m^2, or RV end-systolic volume index ≥80 mL/m^2, or RV end-diastolic volume ≥2× LV end-diastolic volume) aids in the timing of pulmonary valve replacement [45] as discussed in Chap. 4, Born with a Failing Right Heart. RV volumes have shown to be an independent risk factor of cardiac tachyarrhythmia in those patients [46]. Additionally, the function of the RV is a predictor of outcomes in chronic systolic heart failure [47] and non-ischemic dilated cardiomyopathy [48].

3.4.2 Flow Analysis

PC velocity mapping (PC-CMR) is used to analyse blood flow velocity through the cardiac chambers and vessels. In the right side, the peak velocity of TR can be used to calculate the RVSP based on the modified Bernoulli equation, similar to the method used in echocardiography. In the setting of congenital heart disease with PH, CMR allows the quantification of cardiac shunts with the pulmonary-to-systemic flow ratio (Qp:Qs) by performing PC-CMR at the main pulmonary artery and ascending aorta [36], which is an important parameter in the timing of shunt closure. PC-CMR is also able to assess coronary perfusion and identify ischemia of the RV not only in patients with coronary artery disease but also in PH patients [41]. Moreover, the evaluation of the systolic flow in the right coronary artery (RCA) has been reported,

and it is related to RV mass and RV pressure [49]. Intracardiac shunts can also be visualized in a real-time fashion with first-pass perfusion imaging with injection of contrast.

3.4.3 Tissue Characterization

Because of its high definition and ability to characterize myocardial tissue [36], in addition to the quantification of RV volumes, CMR can identify intramyocardial edema and fibrosis, which play an important role in the differential diagnostic work-up of cardiomyopathies. The pattern of fibrosis on DEG imaging can give clues about the differentiation between ischemic and non-ischemic cardiomyopathy. Subendocardial to transmural DEG with a location that is in keeping with an epicardial coronary artery territory is typically described as an ischemic pattern, whereas mid-wall or epicardial DEG (with sparing of the subendocardium) are typically described as a non-ischemic pattern.

Myocardial fibrosis is common in patients with right heart disease; therefore, DEG has an invaluable role in the identification of RV pathology. In patients with PH, DEG located at the right ventricular insertion sites with the interventricular septum (IVS) near the basal segments [50–52] has been related with parameters of RV dysfunction [52]. In Ebstein's anomaly, myocardial fibrosis has been associated with worse clinical status [53].

3.5 The Role of Multi-Detector Computed Tomography

Multi-detector computed tomography (MDCT) is considered the reference standard for anatomical information. Current CT scanners have evolved to more detector rows (up to 128-, 256-, and 320 slice) and dual-source, leading to higher spatial and temporal resolution [54]. This newer generation of scanners has increased the z-axis coverage allowing shorter

breath-hold duration and lower radiation dose, as well as contrast volume with an excellent spatial resolution [55]. However, the images can be suboptimal with fast and irregular cardiac rhythms. MDCT scans include non-contrast high-resolution CT and contrast-enhanced CT angiography (CTA) [56].

Evaluation of volumes and function of the cardiac chambers by CTA involves semiautomated segmentation of the ventricles, using at least ten phases of the cardiac cycle (5–95% phase of the R-R interval) [57, 58]. ECG-gated CTA allows the evaluation of RV function and size, including chamber dilation and wall thickness hypertrophy [59]. The correlation between CT, CMR, and echocardiography modalities has been investigated. MDCT volumes are slightly higher (4%) compared with CMR [32]. Therefore, MDCT is an alternative for the evaluation of RV volumes in patients with devices (cardiac defibrillators or resynchronization therapy) who cannot readily undergo CMR scanning.

Because of its invaluable differentiation of anatomic structures in patients with PH and RV dysfunction, MDCT is most indicated to assess the cardiopulmonary structures in order to investigate the underlying cause of PH (e.g., lung disease, pulmonary embolism, left-to-right shunt as a patent ductus arteriosus or atrial and ventricular septal defect, rheumatologic diseases) and also the secondary changes, allowing for the evaluation of disease severity [60, 61].

In the setting of acute pulmonary embolism, the IVS deviation, RV diameter/LV diameter ratio and the main pulmonary artery diameter (MPAD)/ascending aorta diameter (AOD) ratio evaluated by MDCT can be useful for predicting right ventricular dysfunction [62].

In the new era of percutaneous transcatheter interventions for valvular disease, specifically in TR, multimodality cardiac imaging is a vital component in the selection of the patient and for procedure planning. MDCT is the preferred modality for the anatomic evaluation of the tricuspid annulus, subvalvular apparatus, trabeculations, coronary visualization, vena cava, and femoral venous access, also in addition to right heart size and function [63]. Finally, even though direct quantification

of tricuspid valvular insufficiency is not feasible with CTA, there are anatomical surrogates of valvular regurgitation severity that can be derived, such as the measurement of anatomic regurgitant orifice area during systole and quantification of the tricuspid annular area in diastole [64].

3.6 The Complementary Role of Radionuclide Scan and PET-CT

Radionuclide imaging was the first non-invasive modality for the evaluation of RV function [65]. However, the advent of other non-invasive imaging methods and their technological advances have displaced radionuclide scintigraphy as the first line test in diagnostic work-up. Nevertheless, this technique is able to assess RV function, perfusion, and metabolism, which can provide a comprehensive evaluation of the RV and also be integrated with other non-invasive imaging methods. Through molecular imaging, RV oxygen consumption has been measured with positon emission tomographic (PET) imaging to gain insight onto the pathophysiology of right heart dysfunction [66, 67]; however, the clinical importance of these findings needs to be further assessed.

Case Conclusion

The presented case of a 29-year-old male with diagnosis of secundum ASD shows the important role of multimodal imaging evaluation. The TTE diagnosed the ASD, assessed the RV function, and ruled out PH, which would have been contraindication for the closure of the defect. Next, CMR confirmed the dilation of right heart cavities but still normal RV function, determined significant left-to-right shunting, and visualized the defect from multiple views, providing evidence of feasibility of a percutaneous approach. Tissue characterization showed no ventricular DEG. Additional visualization by both CMR and TOE (Figs. 3.7, 3.8, and 3.9) provided more detailed anatomical information about the defect, complementary imaging of the superior rim, and

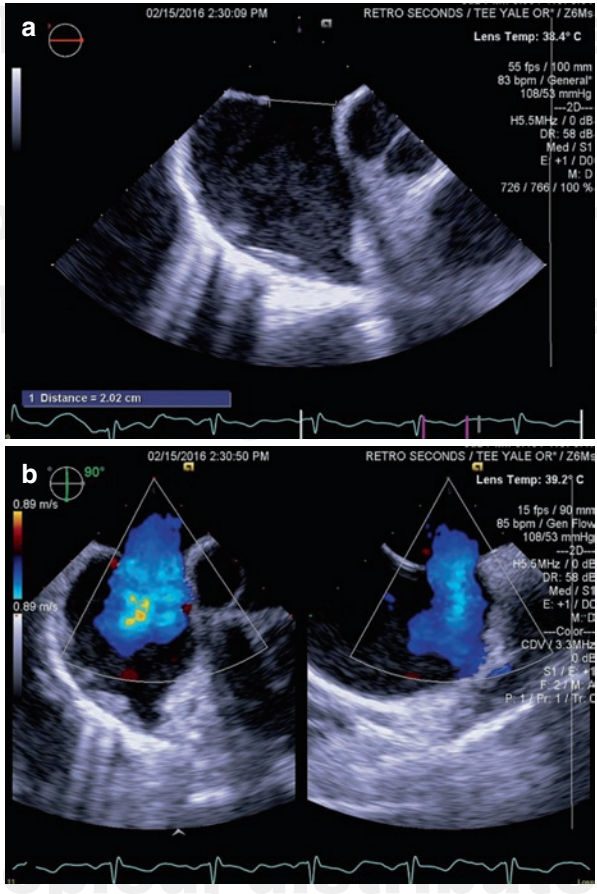

FIGURE 3.7 Transoesophageal echocardiogram (**a**) 2D Mid-oesophageal 0° view showing the ASD measuring 2.0 cm without anterior border. (**b**) 2D colour at mid-oesophageal 0° view showing the flow through the ASD

ruled out any other associated congenital heart disease, in order to provide the highest confidence that the patient was a candidate for percutaneous closure of the defect. Ultimately, the patient underwent successful percutaneous device closure of the defect, avoiding the risks of an open surgery.

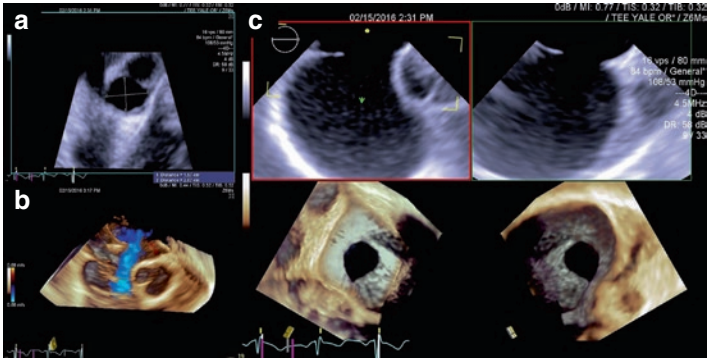

Figure 3.8 Three-dimensional transoesophageal echocardiogram. (**a**) Planimetry of the ASD measuring 2.1 cm in the major diameter and 1.6 cm in the perpendicular diameter. (**b**) 3D short axis at 0° showing the jet trough the ASD. (**c**) 3D short axis at 0° showing the ASD from left atrium (left) and right atrium (right)

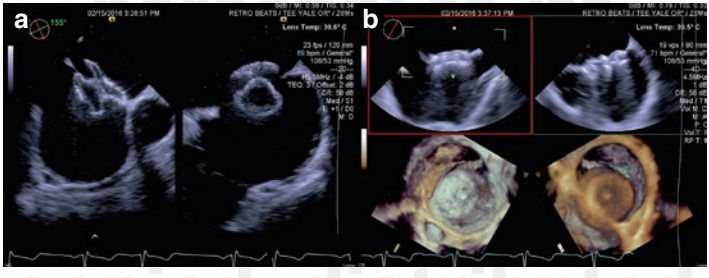

Figure 3.9 Transoesophageal echocardiogram during the ASD closure. (**a**) Bi-plane imaging at 65° and 155° showing when the device is being placed. (**b**) 3D imaging after the deployment of the device from the left atrium (left) and the right atrium (right)

Clinical Pearls

1. The right ventricle has a complex shape and structure, making it challenging to image and assess; as a result, more than one modality may be needed for evaluation.
2. Transthoracic echo remains first-line for cardiac imaging of the right side.

3. Magnetic resonance and transoesophageal echo are often subsequently pursued for complementary information regarding size, function, tissue characterization, and planning for invasive therapeutic procedures.
4. In select cases, additional imaging by computed tomography offers incremental information on structural relationships and procedural planning.
5. Moving forward into the future, emerging and novel parameters of echo and CMR are attempting to further provide new ways to assess the right ventricle as part of diagnostic and prognostic work-up.

References

1. Rudski LG, Lai WW, Afilalo J, Hua L, Handschumacher MD, Chandrasekaran K, et al. Guidelines for the echocardiographic assessment of the right heart in adults: a report from the American Society of Echocardiography endorsed by the European Association of Echocardiography, a registered branch of the European Society of Cardiology, and the Canadian Society of Echocardiography. J Am Soc Echocardiogr. 2010;23(7):685–713.
2. Koifman E, Didier R, Patel N, Jerusalem Z, Kiramijyan S, Ben-Dor I, et al. Impact of right ventricular function on outcome of severe aortic stenosis patients undergoing transcatheter aortic valve replacement. Am Heart J. 2017;184:141–7.
3. Hur DJ, Sugeng L. Non-invasive multimodality cardiovascular imaging of the right heart and pulmonary circulation in pulmonary hypertension. Front Cardiovasc Med. 2019;6:24.
4. Lang RM, Badano LP, Mor-Avi V, Afilalo J, Armstrong A, Ernande L, et al. Recommendations for cardiac chamber quantification by echocardiography in adults: an update from the American Society of Echocardiography and the European Association of Cardiovascular Imaging. J Am Soc Echocardiogr. 2015;28(1):1–39.e14.
5. Genovese D, Mor-Avi V, Palermo C, Muraru D, Volpato V, Kruse E, et al. Comparison between four-chamber and right ventricular-focused views for the quantitative evaluation of right ventricular size and function. J Am Soc Echocardiogr. 2019;32(4):484–94.

6. Gleason WL, Braunwald E. Studies on the first derivative of the ventricular pressure pulse in man. J Clin Invest. 1962;41:80–91.
7. Anconina J, Danchin N, Selton-Suty C, Isaaz K, Juilliere Y, Buffet P, et al. Noninvasive estimation of right ventricular dP/dt in patients with tricuspid valve regurgitation. Am J Cardiol. 1993;71(16):1495–7.
8. Sade LE, Gulmez O, Eroglu S, Sezgin A, Muderrisoglu H. Noninvasive estimation of right ventricular filling pressure by ratio of early tricuspid inflow to annular diastolic velocity in patients with and without recent cardiac surgery. J Am Soc Echocardiogr. 2007;20(8):982–8.
9. Sundereswaran L, Nagueh SF, Vardan S, Middleton KJ, Zoghbi WA, Quinones MA, et al. Estimation of left and right ventricular filling pressures after heart transplantation by tissue Doppler imaging. Am J Cardiol. 1998;82(3):352–7.
10. Thenappan T, Shah SJ, Rich S, Tian L, Archer SL, Gomberg-Maitland M. Survival in pulmonary arterial hypertension: a reappraisal of the NIH risk stratification equation. Eur Respir J. 2010;35(5):1079–87.
11. Gan CT, Holverda S, Marcus JT, Paulus WJ, Marques KM, Bronzwaer JG, et al. Right ventricular diastolic dysfunction and the acute effects of sildenafil in pulmonary hypertension patients. Chest. 2007;132(1):11–7.
12. Dell'Italia LJ. The right ventricle: anatomy, physiology, and clinical importance. Curr Probl Cardiol. 1991;16(10):653–720.
13. Kawel-Boehm N, Maceira A, Valsangiacomo-Buechel ER, Vogel-Claussen J, Turkbey EB, Williams R, et al. Normal values for cardiovascular magnetic resonance in adults and children. J Cardiovasc Magn Reson. 2015;17:29.
14. Naeije R, Badagliacca R. The overloaded right heart and ventricular interdependence. Cardiovasc Res. 2017;113(12):1474–85.
15. Buckberg G, Hoffman JI, Mahajan A, Saleh S, Coghlan C. Cardiac mechanics revisited: the relationship of cardiac architecture to ventricular function. Circulation. 2008;118(24):2571–87.
16. Kaminska M, Sobkowicz B, Sawicki R, Lewkowicz J, Tomaszuk-Kazberuk A, Glinska R, et al. Is real time contrast echocardiography useful for assessment of the right ventricular morphology, function, and perfusion? Echocardiography. 2015;32(7):1080–6.
17. Medvedofsky D, Mor-Avi V, Kruse E, Guile B, Ciszek B, Weinert L, et al. Quantification of right ventricular size and function from contrast-enhanced three-dimensional echocardiographic images. J Am Soc Echocardiogr. 2017;30(12):1193–202.

18. Badano LP, Kolias TJ, Muraru D, Abraham TP, Aurigemma G, Edvardsen T, et al. Standardization of left atrial, right ventricular, and right atrial deformation imaging using two-dimensional speckle tracking echocardiography: a consensus document of the EACVI/ASE/industry task force to standardize deformation imaging. Eur Heart J Cardiovasc Imaging. 2018;19(6):591–600.
19. Sanz-de la Garza M, Giraldeau G, Marin J, Imre Sarvari S, Guasch E, Gabrielli L, et al. Should the septum be included in the assessment of right ventricular longitudinal strain? An ultrasound two-dimensional speckle-tracking stress study. Int J Cardiovasc Imaging. 2019;35:1853–60.
20. Mor-Avi V, Lang RM, Badano LP, Belohlavek M, Cardim NM, Derumeaux G, et al. Current and evolving echocardiographic techniques for the quantitative evaluation of cardiac mechanics: ASE/EAE consensus statement on methodology and indications endorsed by the Japanese Society of Echocardiography. Eur J Echocardiogr. 2011;12(3):167–205.
21. Negishi K, Negishi T, Kurosawa K, Hristova K, Popescu BA, Vinereanu D, et al. Practical guidance in echocardiographic assessment of global longitudinal strain. JACC Cardiovasc Imaging. 2015;8(4):489–92.
22. Verhaert D, Mullens W, Borowski A, Popovic ZB, Curtin RJ, Thomas JD, et al. Right ventricular response to intensive medical therapy in advanced decompensated heart failure. Circ Heart Fail. 2010;3(3):340–6.
23. Guendouz S, Rappeneau S, Nahum J, Dubois-Rande JL, Gueret P, Monin JL, et al. Prognostic significance and normal values of 2D strain to assess right ventricular systolic function in chronic heart failure. Circ J. 2012;76(1):127–36.
24. Houard L, Benaets MB, de Meester de Ravenstein C, Rousseau MF, Ahn SA, Amzulescu MS, et al. Additional prognostic value of 2D right ventricular speckle-tracking strain for prediction of survival in heart failure and reduced ejection fraction: a comparative study with cardiac magnetic resonance. JACC Cardiovasc Imaging. 2019;12(12):2373–85.
25. Antoni ML, Scherptong RW, Atary JZ, Boersma E, Holman ER, van der Wall EE, et al. Prognostic value of right ventricular function in patients after acute myocardial infarction treated with primary percutaneous coronary intervention. Circ Cardiovasc Imaging. 2010;3(3):264–71.
26. Ivey-Miranda JB, Almeida-Gutierrez E, Borrayo-Sanchez G, Antezana-Castro J, Contreras-Rodriguez A, Posada-Martinez

EL, et al. Right ventricular longitudinal strain predicts acute kidney injury and short-term prognosis in patients with right ventricular myocardial infarction. Int J Cardiovasc Imaging. 2019;35(1):107–16.

27. Borges AC, Knebel F, Eddicks S, Panda A, Schattke S, Witt C, et al. Right ventricular function assessed by two-dimensional strain and tissue Doppler echocardiography in patients with pulmonary arterial hypertension and effect of vasodilator therapy. Am J Cardiol. 2006;98(4):530–4.
28. Bartko PE, Wiedemann D, Schrutka L, Binder C, Santos-Gallego CG, Zuckermann A, et al. Impact of right ventricular performance in patients undergoing extracorporeal membrane oxygenation following cardiac surgery. J Am Heart Assoc. 2017;6(8):e005455.
29. Ternacle J, Berry M, Cognet T, Kloeckner M, Damy T, Monin JL, et al. Prognostic value of right ventricular two-dimensional global strain in patients referred for cardiac surgery. J Am Soc Echocardiogr. 2013;26(7):721–6.
30. Peyrou J, Chauvel C, Pathak A, Simon M, Dehant P, Abergel E. Preoperative right ventricular dysfunction is a strong predictor of 3 years survival after cardiac surgery. Clin Res Cardiol. 2017;106(9):734–42.
31. Geva T, Powell AJ, Crawford EC, Chung T, Colan SD. Evaluation of regional differences in right ventricular systolic function by acoustic quantification echocardiography and cine magnetic resonance imaging. Circulation. 1998;98(4):339–45.
32. Sugeng L, Mor-Avi V, Weinert L, Niel J, Ebner C, Steringer-Mascherbauer R, et al. Multimodality comparison of quantitative volumetric analysis of the right ventricle. JACC Cardiovasc Imaging. 2010;3(1):10–8.
33. Nagata Y, Wu VC, Kado Y, Otani K, Lin FC, Otsuji Y, et al. Prognostic value of right ventricular ejection fraction assessed by transthoracic 3D echocardiography. Circ Cardiovasc Imaging. 2017;10(2):e005384.
34. Ryo K, Goda A, Onishi T, Delgado-Montero A, Tayal B, Champion HC, et al. Characterization of right ventricular remodeling in pulmonary hypertension associated with patient outcomes by 3-dimensional wall motion tracking echocardiography. Circ Cardiovasc Imaging. 2015;8(6):e003176.
35. Hundley WG, Bluemke DA, Finn JP, Flamm SD, Fogel MA, Friedrich MG, et al. ACCF/ACR/AHA/NASCI/SCMR 2010

expert consensus document on cardiovascular magnetic resonance: a report of the American College of Cardiology Foundation Task Force on Expert Consensus Documents. J Am Coll Cardiol. 2010;55(23):2614–62.

36. Pena E, Dennie C, Veinot J, Muniz SH. Pulmonary hypertension: how the radiologist can help. Radiographics. 2012;32(1):9–32.
37. Haddad F, Hunt SA, Rosenthal DN, Murphy DJ. Right ventricular function in cardiovascular disease, part I: anatomy, physiology, aging, and functional assessment of the right ventricle. Circulation. 2008;117(11):1436–48.
38. Peacock AJ, Vonk Noordegraaf A. Cardiac magnetic resonance imaging in pulmonary arterial hypertension. Eur Respir Rev. 2013;22(130):526–34.
39. Marrone G, Mamone G, Luca A, Vitulo P, Bertani A, Pilato M, et al. The role of 1.5T cardiac MRI in the diagnosis, prognosis and management of pulmonary arterial hypertension. Int J Cardiovasc Imaging. 2010;26(6):665–81.
40. McMurray JJ, Adamopoulos S, Anker SD, Auricchio A, Bohm M, Dickstein K, et al. ESC guidelines for the diagnosis and treatment of acute and chronic heart failure 2012: the task force for the diagnosis and treatment of acute and chronic heart failure 2012 of the European Society of Cardiology. Developed in collaboration with the heart failure association (HFA) of the ESC. Eur J Heart Fail. 2012;14(8):803–69.
41. Freed BH, Collins JD, Francois CJ, Barker AJ, Cuttica MJ, Chesler NC, et al. MR and CT imaging for the evaluation of pulmonary hypertension. JACC Cardiovasc Imaging. 2016;9(6):715–32.
42. McLure LE, Peacock AJ. Cardiac magnetic resonance imaging for the assessment of the heart and pulmonary circulation in pulmonary hypertension. Eur Respir J. 2009;33(6):1454–66.
43. Alunni JP, Degano B, Arnaud C, Tetu L, Blot-Souletie N, Didier A, et al. Cardiac MRI in pulmonary artery hypertension: correlations between morphological and functional parameters and invasive measurements. Eur Radiol. 2010;20(5):1149–59.
44. Aquaro GD, Pingitore A, Di Bella G, Piaggi P, Gaeta R, Grigoratos C, et al. Prognostic role of cardiac magnetic resonance in arrhythmogenic right ventricular cardiomyopathy. Am J Cardiol. 2018;122(10):1745–53.
45. Stout KK, Daniels CJ, Aboulhosn JA, Bozkurt B, Broberg CS, Colman JM, et al. 2018 AHA/ACC guideline for the management of adults with congenital heart disease: a report of the American College of Cardiology/American Heart Association

Task Force on clinical practice guidelines. J Am Coll Cardiol. 2019;73(12):e81–e192.
46. Beurskens NEG, Hagdorn QAJ, Gorter TM, Berger RMF, Vermeulen KM, van Melle JP, et al. Risk of cardiac tachyarrhythmia in patients with repaired tetralogy of Fallot: a multicenter cardiac MRI based study. Int J Cardiovasc Imaging. 2019;35(1):143–51.
47. Meyer P, Filippatos GS, Ahmed MI, Iskandrian AE, Bittner V, Perry GJ, et al. Effects of right ventricular ejection fraction on outcomes in chronic systolic heart failure. Circulation. 2010;121(2):252–8.
48. Gulati A, Ismail TF, Jabbour A, Alpendurada F, Guha K, Ismail NA, et al. The prevalence and prognostic significance of right ventricular systolic dysfunction in nonischemic dilated cardiomyopathy. Circulation. 2013;128(15):1623–33.
49. van Wolferen SA, Marcus JT, Westerhof N, Spreeuwenberg MD, Marques KM, Bronzwaer JG, et al. Right coronary artery flow impairment in patients with pulmonary hypertension. Eur Heart J. 2008;29(1):120–7.
50. Blyth KG, Groenning BA, Martin TN, Foster JE, Mark PB, Dargie HJ, et al. Contrast enhanced-cardiovascular magnetic resonance imaging in patients with pulmonary hypertension. Eur Heart J. 2005;26(19):1993–9.
51. McCann GP, Gan CT, Beek AM, Niessen HW, Vonk Noordegraaf A, van Rossum AC. Extent of MRI delayed enhancement of myocardial mass is related to right ventricular dysfunction in pulmonary artery hypertension. AJR Am J Roentgenol. 2007;188(2):349–55.
52. Swift AJ, Rajaram S, Capener D, Elliot C, Condliffe R, Wild JM, et al. LGE patterns in pulmonary hypertension do not impact overall mortality. JACC Cardiovasc Imaging. 2014;7(12):1209–17.
53. Yang D, Li X, Sun JY, Cheng W, Greiser A, Zhang TJ, et al. Cardiovascular magnetic resonance evidence of myocardial fibrosis and its clinical significance in adolescent and adult patients with Ebstein's anomaly. J Cardiovasc Magn Reson. 2018;20(1):69.
54. Sun Z, Choo GH, Ng KH. Coronary CT angiography: current status and continuing challenges. Br J Radiol. 2012;85(1013):495–510.
55. Lewis MA, Pascoal A, Keevil SF, Lewis CA. Selecting a CT scanner for cardiac imaging: the heart of the matter. Br J Radiol. 2016;89(1065):20160376.

56. Galie N, Humbert M, Vachiery JL, Gibbs S, Lang I, Torbicki A, et al. 2015 ESC/ERS guidelines for the diagnosis and treatment of pulmonary hypertension: the joint task force for the diagnosis and treatment of pulmonary hypertension of the European Society of Cardiology (ESC) and the European Respiratory Society (ERS): endorsed by: Association for European Paediatric and Congenital Cardiology (AEPC), International Society for Heart and Lung Transplantation (ISHLT). Eur Respir J. 2015;46(4):903–75.
57. Henneman MM, Schuijf JD, Jukema JW, Holman ER, Lamb HJ, de Roos A, et al. Assessment of global and regional left ventricular function and volumes with 64-slice MSCT: a comparison with 2D echocardiography. J Nucl Cardiol. 2006;13(4):480–7.
58. Greupner J, Zimmermann E, Grohmann A, Dubel HP, Althoff TF, Borges AC, et al. Head-to-head comparison of left ventricular function assessment with 64-row computed tomography, biplane left cineventriculography, and both 2- and 3-dimensional transthoracic echocardiography: comparison with magnetic resonance imaging as the reference standard. J Am Coll Cardiol. 2012;59(21):1897–907.
59. Abel E, Jankowski A, Pison C, Luc Bosson J, Bouvaist H, Ferretti GR. Pulmonary artery and right ventricle assessment in pulmonary hypertension: correlation between functional parameters of ECG-gated CT and right-side heart catheterization. Acta Radiol. 2012;53(7):720–7.
60. Ceriani E, Combescure C, Le Gal G, Nendaz M, Perneger T, Bounameaux H, et al. Clinical prediction rules for pulmonary embolism: a systematic review and meta-analysis. J Thromb Haemost. 2010;8(5):957–70.
61. Mesquita SM, Castro CR, Ikari NM, Oliveira SA, Lopes AA. Likelihood of left main coronary artery compression based on pulmonary trunk diameter in patients with pulmonary hypertension. Am J Med. 2004;116(6):369–74.
62. Jia D, Zhou XM, Hou G. Estimation of right ventricular dysfunction by computed tomography pulmonary angiography: a valuable adjunct for evaluating the severity of acute pulmonary embolism. J Thromb Thrombolysis. 2017;43(2):271–8.
63. Khalique OK, Cavalcante JL, Shah D, Guta AC, Zhan Y, Piazza N, et al. Multimodality imaging of the tricuspid valve and right heart anatomy. JACC Cardiovasc Imaging. 2019;12(3):516–31.

64. Hahn RT, Thomas JD, Khalique OK, Cavalcante JL, Praz F, Zoghbi WA. Imaging assessment of tricuspid regurgitation severity. JACC Cardiovasc Imaging. 2019;12(3):469–90.
65. Rich JD, Ward RP. Right-ventricular function by nuclear cardiology. Curr Opin Cardiol. 2010;25(5):445–50.
66. Wong YY, Ruiter G, Lubberink M, Raijmakers PG, Knaapen P, Marcus JT, et al. Right ventricular failure in idiopathic pulmonary arterial hypertension is associated with inefficient myocardial oxygen utilization. Circ Heart Fail. 2011;4(6):700–6.
67. Wong YY, Raijmakers P, van Campen J, van der Laarse WJ, Knaapen P, Lubberink M, et al. 11C-Acetate clearance as an index of oxygen consumption of the right myocardium in idiopathic pulmonary arterial hypertension: a validation study using 15O-labeled tracers and PET. J Nucl Med. 2013;54(8):1258–62.